

## The Morphology of Vesicles of Higher Topological Genus: Conformal Degeneracy and Conformal Modes

Frank Jülicher (\*)

Institut für Festkörperforschung, Forschungszentrum Jülich, 52425 Jülich, Germany

and

Department of Physics, Simon Fraser University, Burnaby, British Columbia V5A 1S6, Canada

(Received 5 July 1996, accepted 27 August 1996)

PACS.82.70.-y – Disperse systems

PACS.02.40.-k – Geometry, differential geometry, and topology

**Abstract.** — The morphology of vesicles with topological genus  $g = 2$  is studied using the properties of Willmore surfaces together with the conformal invariance of the bending energy of fluid membranes. In the phase diagram of the bilayer couple model, a region exists where vesicle shapes are given by Willmore surfaces. Within this region, shapes in general have no mirror symmetries and the ground state is conformally degenerate. The conformal modes which correspond to this degeneracy can be described as closed curves in a three-dimensional space. The existence of conformal modes leads to unusual shape fluctuations which correspond to a diffusion process in shape space called conformal diffusion. Additional regions exist in the phase diagram where the ground state is unique and vesicle shapes have two or more mirror planes. Conformal degeneracy and conformal diffusion also exist in the area-difference-elasticity model.

### 1. Introduction

Lipids are amphiphilic molecules which can be dissolved in an aqueous environment where they self-assemble and form two-dimensional bilayers or membranes [1, 2]. In order to avoid the exposure of hydrophobic tails of the lipid molecules with water, a membrane tends to form closed surfaces or vesicles. Vesicles can be observed experimentally under the microscope. Their observation reveals a rich variety of different shapes [3–6]. Curvature models which are based on the assumption that vesicle shapes are determined by the bending elasticity of the membranes [7, 8] allow the theoretical study of these shapes [9–14].

Vesicles can also be classified by their topology. The topology of a vesicle is characterized by its topological genus  $g$  which counts the number of “handles” that have to be attached to a sphere to obtain a surface of given topology. Vesicles with the topology of a sphere, *i.e.*  $g = 0$ , are most common. However, vesicles with toroidal topology, *i.e.*  $g = 1$  [15–17], and vesicles with two, three and even more “handles” [18, 19] have been observed experimentally.

The bending energy of fluid membranes is invariant under conformal transformations of the shape [20, 21]. Theoretical studies show that this invariance has physical significance for

---

(\*) *Present address:* Institut Curie, Section de Recherche, 11 rue Pierre et Marie Curie, 75231 Paris, Cedex 05, France (e-mail: Frank.Julicher@curie.fr)

vesicles of non-spherical topology [21–27]. In particular, it was predicted theoretically that the shape of vesicles of topological genus  $g > 1$  can be conformally degenerate. This degeneracy leads to a novel type of shape fluctuations called conformal diffusion [27]. The experimental observation of this phenomenon has been reported recently [19].

The morphology of vesicles of genus  $g > 1$  is closely linked to the properties of Willmore surfaces. As described in the mathematical literature, Willmore surfaces can be obtained as stereo-graphic images of minimal surfaces embedded in the four-dimensional unit sphere  $S^3$  [28–32]. Different examples of such minimal surfaces have been discovered in the last decades [33, 34]. The properties of Willmore surfaces together with the conformal invariance of the bending energy allows to determine phase diagrams for vesicle shapes and to study conformal modes which occur if vesicle shapes are conformally degenerate.

The purpose of this paper is to present a detailed study of the morphology of genus-2 vesicles. After defining curvature models for vesicle shapes in Section 2, Willmore surfaces and their relevance for the physics of vesicle shapes are introduced in Section 3. A complete classification of genus-2 Willmore surfaces is given in Section 4. As described in Section 5, Willmore surfaces are solutions to curvature models for vesicle shapes within a certain region of the phase diagram. The existence of the conformal degeneracy of the ground-state is shown in Section 6 and the structure of conformal modes is analyzed. Phase diagrams of vesicle shapes are described in Section 7. The paper ends with a description of recent experiments and a discussion. The appendix reviews the conformal invariance of the bending energy and the relation between Willmore surfaces and minimal surfaces. Numerical methods used in this paper are described. Some of these results have been reported previously in reference [27].

## 2. Curvature Models for Vesicle Shapes

The bending energy of a homogeneous membrane which is symmetric with respect to its two monolayers can be written as [7, 8]

$$F \equiv \frac{\kappa}{2} \oint dA (2H)^2 + \kappa_G \oint dA K \quad . \quad (1)$$

Here,  $dA$  is the area element on the surface,  $H$  and  $K$  are the mean and Gaussian curvatures as defined in Appendix A. The bending rigidity  $\kappa$  and the Gaussian bending modulus  $\kappa_G$  describe the elastic properties of the membrane.

A vesicle attains a shape which is the minimum of the bending energy (1) taking into account physical constraints: First, for an incompressible membrane, the area  $A$  is fixed since it is determined by the number of lipid molecules in the membrane. Furthermore, the volume  $V$  which is enclosed by the membrane is fixed by osmotic conditions: An in-flux or out-flux of water would lead to a buildup of osmotic pressures which oppose this flux.

For vesicle shape calculations, the Gaussian curvature contribution to the bending energy is irrelevant. This fact follows from the Gauss-Bonnet theorem which states that the area-integral over the Gaussian curvature is a topological invariant, see Appendix A.5. Since the bending energy  $F$  is minimized for fixed topology, the Gaussian curvature term leads to a constant contribution which can be omitted. Therefore only the energy

$$G \equiv \frac{\kappa}{2} \oint dA (2H)^2 \quad (2)$$

is minimized.

2.1. THE BILAYER COUPLE MODEL. — A membrane consists of two monolayers which form a bilayer. This bilayer structure is relevant for the vesicle shape since the flip-flop of lipid molecules between both monolayers is strongly suppressed and the number of lipids in each individual monolayer is constant. In the bilayer couple model (BC-model) [10,11], it is assumed that both monolayers are incompressible. As a result, the difference

$$\Delta A \equiv A^{\text{ex}} - A^{\text{in}} \simeq 2dM \quad (3)$$

of the areas of the outer and the inner monolayers  $A^{\text{ex}}$  and  $A^{\text{in}}$  is fixed. This area difference is proportional to the separation  $d$  of the neutral surfaces in the monolayers and to the total mean curvature

$$M \equiv \oint dAH \quad . \quad (4)$$

The bending energy (2) is scale invariant and only depends on the shape of a vesicle. Therefore, two dimensionless parameters characterize a vesicle: The reduced volume

$$v \equiv \frac{3V}{4\pi R_0^3} \quad , \quad (5)$$

and the reduced total mean curvature

$$m \equiv \frac{M}{R_0} \quad , \quad (6)$$

where  $4\pi R_0^2 = A$ .

In the BC-model, a vesicle shape of given topology is determined as the shape of minimal bending energy  $G$  given the values  $v$  and  $m$  of the reduced volume and the reduced total mean curvature.

2.2. THE AREA-DIFFERENCE ELASTICITY MODEL. — A more realistic model for vesicle shapes is the area-difference elasticity model (ADE-model) [6,13]. In this model, the monolayers have finite compressibility. As a result, the constraint on the total mean curvature  $m$  is replaced by an elastic energy which occurs if  $m$  deviates from a relaxed value  $m_0$  for which the monolayers are not compressed. The total energy reads

$$W \equiv G + \frac{\kappa\alpha}{2}(m - m_0)^2 \quad , \quad (7)$$

where  $\alpha$  is a dimensionless parameter which characterizes the membrane. In the ADE-model, a vesicle shape is given by the minimum of the energy (7) for fixed reduced volume  $v$  and fixed relaxed total mean curvature  $m_0$ .

### 3. The Willmore Problem

In 1965, Willmore proposed a geometrical problem which later was called the “Willmore problem” [20,28,35]. The problem is to find the surface which corresponds to the minimum of the functional

$$\frac{G}{2\kappa} = \oint dA H^2 \quad , \quad (8)$$

for given topological genus  $g$ . A surface with this property is called a Willmore surface. Willmore surfaces are therefore shapes of minimal bending energy  $G$ . However, they are pure geometrical objects since no physical constraints are imposed.

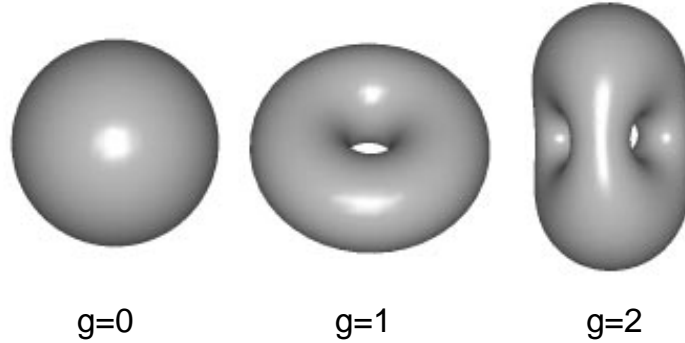


Fig. 1. — Willmore surfaces for different topological genus  $g$ . The sphere for  $g = 0$ , the Clifford torus for  $g = 1$  and the genus-2 Lawson surface.

Willmore showed that for spherical topology, or  $g = 0$ , the solution is the sphere with  $G = G_0 \equiv 8\pi\kappa$ . Furthermore, he could prove that  $G \geq 8\pi\kappa$ , which implies that the absolute minimum with respect to all topologies is obtained for a sphere. For toroidal topology, or  $g = 1$ , Willmore conjectured that the so-called Clifford torus minimizes (8) with  $G = G_1 \equiv \pi G_0/2$  [20]. The Clifford torus is an axisymmetric torus with circular cross-section (see Fig. 1). It is defined by a ratio of  $2^{1/2}$  of the radii of the two generating circles. It is interesting to note that no general proof for Willmore's conjecture is known.

An important property of the Willmore functional (8) is its conformal invariance [20, 31]: As reviewed in Appendix A.2, the value of  $G$  does not change if a surface is deformed by conformal transformations in three dimensional space. Conformal transformations which deform the shape change of a given surface can be generated by using inversions  $\mathbf{R}' = \mathbf{R}/R^2$  and translations by a vector  $\mathbf{a} = (a_X, a_Y, a_Z)$ . It is most convenient to use special conformal transformations (SCT) which consist of an inversion followed by a translation and a second inversion. A SCT thus maps a point  $\mathbf{R}$  to [36]

$$\mathbf{R}' = \frac{\mathbf{R}/R^2 - \mathbf{a}}{(\mathbf{R}/R^2 - \mathbf{a})^2} \quad (9)$$

As a consequence of the conformal invariance of  $G$ , the solutions of the Willmore problem are degenerate since SCT's applied to a Willmore surface generate new Willmore surfaces of the same topology.

For spherical topology, however, the sphere is the unique solution which is not deformed by conformal transformations. For toroidal topology there exists a one-dimensional family of non-axisymmetric Willmore surfaces which can be generated from the Clifford torus by applying SCT's. The existence of a whole family of genus-1 Willmore surfaces has physical consequences for vesicles of toroidal topology [25, 26]. In particular, it leads to the existence of regions with non-axisymmetric shapes in the phase diagrams of different curvature models [26].

3.1. WILLMORE SURFACES AS MINIMAL SURFACES IN  $S^3$ . — Willmore surfaces of topological genus  $g > 1$  can be discussed using an important property of Willmore surfaces, namely their relation to minimal surfaces embedded in the four dimensional unit sphere  $S^3$  [28, 30–32]. This relation can be summarized as follows: An arbitrary closed surface in  $S^3$  can be mapped by a stereo-graphic projection into the three dimensional Euclidean space  $R^3$ , see Appendix A.3 and A.4 for details. This stereo-graphic projection has special properties if the original surface

is a minimal surface in  $S^3$ : The stereo-graphic image of such a minimal surface is a stationary solution of the Willmore functional with

$$G = 2\kappa\tilde{A} \quad \text{and} \quad \delta G = 0 \quad . \tag{10}$$

Here,  $\tilde{A}$  is the surface area of the minimal surface in  $S^3$ . A derivation of equation (10) is given in Appendix C.

The argument outlined above cannot be reversed. There could exist surfaces with  $\delta G = 0$  which are not the stereo-graphic image of a minimal surface. However, equation (10) implies that if a Willmore surface is the projected image of a minimal surface, this minimal surface has the smallest surface area  $\hat{A}$  compared to other minimal surfaces with the same topological genus.

On order to find solutions to the Willmore problem, the mathematician Kusner compared upper bounds for the surface areas  $\hat{A}$  of different minimal surfaces which had been discovered by Lawson [33]. This comparison led him to conjecture that the Willmore surface of topological genus  $g$  is given by the stereo-graphic image of a minimal surface  $\xi_{1g}$  [30]. A brief discussion of minimal surfaces in  $S^3$  is given in Appendix B.

Hsu, Kusner and Sullivan checked Kusner’s conjecture for  $g \leq 5$  by numerically minimizing  $G$  [29]. Their results strongly support this conjecture. Kusner’s conjecture is a generalization of Willmore’s conjecture since it includes the sphere and the Clifford torus as special cases for  $g = 0$  and  $g = 1$ . For  $g > 1$ , however, there exist no analytic expressions for the minimal surfaces  $\xi_{1g}$  which define the corresponding Willmore surfaces *via* stereo-graphic projections.

The stereo-graphic images of the surfaces  $\xi_{1g}$  are not unique. Rotating the three-dimensional unit sphere  $S^3$  in  $R^4$  leads to different projections in  $R^3$  which are Willmore surfaces with the same minimal value of  $G$ . These surfaces are related by conformal transformations, thus reflecting the conformal invariance of the Willmore functional. For given topological genus  $g$ , there exists exactly one stereo-graphic projection which reveals all the symmetry properties of the original surface in  $S^3$ . This surface in  $R^3$  which is the most symmetric Willmore surface, is in the following called *Lawson surface* of genus  $g$ .

3.2. THE GENUS-2 LAWSON SURFACE. — The genus-2 Lawson surface  $L$  is shown in Figure 2. It is  $\mathcal{D}_{3h}$ -symmetric, using the Schönflies notation for symmetry groups [37]: It has a three-fold symmetry axis, three mirror planes that contain this axis and one mirror plane perpendicular to the symmetry axis. In the following, a coordinate system  $\mathbf{R} = (X, Y, Z)$  will be used with  $Z$ -axis given by the three-fold symmetry axis and an  $X$ - $Y$ -plane defined by the mirror plane perpendicular to this axis.

In addition to these mirror symmetries, the Lawson surface is invariant under inversions  $\mathbf{R}' = \lambda^2\mathbf{R}/R^2$  at a sphere with radius  $\lambda$ . The radius  $\lambda$  is determined by the condition that the sphere cuts  $L$  perpendicular and can be chosen arbitrarily by rescaling of  $L$ . This sphere is in the following called the “sphere of inversion symmetry”. This sphere together with the mirror planes of  $L$  will be called “symmetry surfaces” of  $L$ . The symmetry properties of  $L$  are a result of the symmetries of the minimal surface  $\xi_{12}$ . The mirror planes and also the inversion symmetry of  $L$  correspond to reflection symmetries of the minimal surface  $\xi_{12}$  in  $R^4$ .

The genus-2 Lawson surface can be approximated numerically by minimizing a discretized version of the functional  $G$  for a triangulated surface of topological genus  $g = 2$ . The surface shown in Figure 2 has been obtained by this method which is described in Appendix D. This surface consists of  $n_T = 24576$  triangles,  $n_E = 36864$  edges and  $n_V = 12286$  vertices. It has the reduced volume  $v \simeq 0.677$  and the reduced total mean curvature  $m \simeq 1.037$ . The bending energy is  $G = G_2 \simeq (1.75 \pm 0.01) \cdot 8\pi\kappa$ . This value is in close agreement with the result of Hsu, Kusner and Sullivan [29].

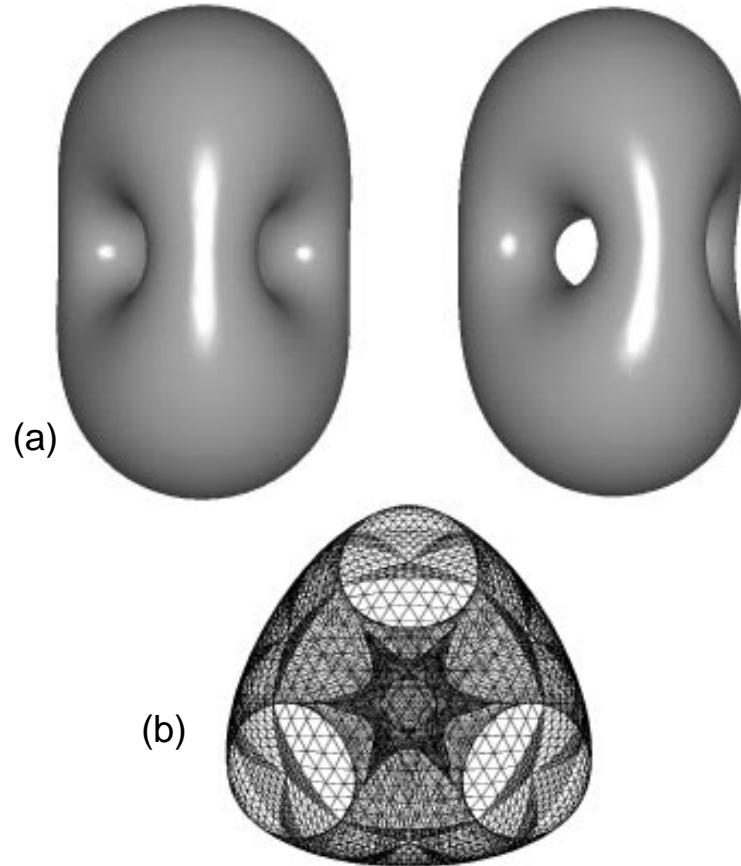


Fig. 2. — (a) Two views of the  $\mathcal{D}_{3h}$ -symmetric Lawson surface  $L$  for topological genus  $g = 2$ . This surface was generated by numerically minimizing a discretized version of the bending energy  $G$ . (b) A projection of the triangulation used to represent the surface on the  $X$ - $Y$ -plane.

#### 4. Classification of Conformally Degenerate Willmore Surfaces

Willmore surfaces of topological genus  $g = 2$  can be obtained by applying special conformal transformations to the Lawson surface  $L$ . The complete set of conformally degenerate Willmore surfaces with  $g = 2$  is denoted  $\mathcal{W}_2$ . Willmore surfaces of  $\mathcal{W}_2$  can be classified in different families. The structure of  $\mathcal{W}_2$  and the symmetries of surfaces within different families is related to the structure and the symmetries of the Lawson surface.

4.1. PARAMETERIZATION OF WILLMORE SURFACES. — The invariance of the Lawson surface  $L$  with respect to inversions leads to a simplification of SCT's applied to  $L$ . The first inversion in equation (9) can be omitted and the simplified transformation reads

$$\mathbf{R}' = \frac{\mathbf{R} - \mathbf{a}}{(\mathbf{R} - \mathbf{a})^2} \quad . \quad (11)$$

Equation (11) corresponds to a single inversion centered at the point  $\mathbf{a}$ .

A conformal transformation as given by equation (11) defines a mapping of  $L$  to a Willmore surface. Each Willmore surface can be uniquely identified by the inversion center  $\mathbf{a}$  used for its generation. This provides a parameterization of the set  $\mathcal{W}_2$  of Willmore surfaces by a vector  $\mathbf{a} = (a_X, a_Y, a_Z)$ . In this parameterization, the Lawson surface corresponds to  $\mathbf{a} = (0, 0, 0)$ . All remaining Willmore surfaces correspond to different points  $\mathbf{a}$  in  $R^3$ . Therefore,  $\mathcal{W}_2$  is a three-dimensional space.

4.2. SINGULAR WILLMORE SURFACES. — Singular Willmore surfaces occur for inversion centers  $\mathbf{a}$  for which the transformation (11) becomes singular. This happens if  $\mathbf{a}$  coincides with a point  $\mathbf{R}$  of the Lawson surface  $L$ . In this case, the inversion (11) generates a limit shape which can be well defined if the generated surface is rescaled in order to keep the surface area  $A$  finite. If  $\mathbf{a}$  approaches a surface point of  $L$ , a limit shape  $S$  is generated which consists of a sphere with an infinitesimal handle attached in one point [38].

Any point of the Lawson surface defines such a limit shape. As a consequence, a two-dimensional set of limit shapes  $S$  exists which corresponds to points  $\mathbf{a}$  of the Lawson surface  $L$ . All points  $\mathbf{a}$  located in the interior of  $L$  lead to nonsingular Willmore surfaces [39]. The Lawson surface therefore defines the boundary of the parameterization and thus the boundary of  $\mathcal{W}_2$ . The fact that the boundary of  $\mathcal{W}_2$  itself has the shape of the Lawson surface indicates that the topology of  $\mathcal{W}_2$  is nontrivial.

4.3. FAMILIES OF WILLMORE SURFACES. — Willmore surfaces in  $\mathcal{W}_2$  can be classified by their symmetries. The Lawson surface  $L$  is the most symmetric Willmore surface. Inversions applied to  $L$  break some or all of the mirror symmetries of  $L$ . First, consider inversions with  $\mathbf{a}$  located in the  $X$ - $Y$ -plane, *i.e.*  $\mathbf{a} = (a_X, a_Y, 0)$ . The corresponding Willmore surfaces are mirror-symmetric with respect to the  $X$ - $Y$ -plane. In order to understand the additional symmetries of these Willmore surfaces, it is sufficient to study the transformation of the cross-section of  $L$  with the  $X$ - $Y$ -plane under inversions at a circle centered at  $(a_X, a_Y)$ .

The cross-section of  $L$  consists of three identical pieces which are slightly deformed circles, see Figure 2b. For simplicity, a model for  $L$  as displayed in Figure 3a is discussed, where the cross-section of  $L$  with the  $X$ - $Y$ -plane is approximated by circles. This model consists of three circles of equal radii which are centered at the vertices of an equilateral triangle. This arrangement of circles has threefold symmetry and, as a result of a proper choice of the radii of these circles, it is invariant with respect to an inversion at a unit circle. This circle of inversion symmetry is indicated in Figure 3a by a broken line.

Conformal transformations on the Lawson surface with  $\mathbf{a} = (a_X, a_Y, 0)$  located in the  $X$ - $Y$ -plane now correspond to conformal transformations of this structure. A circle  $C$  with radius  $r$  and center  $\mathbf{m}$  is transformed by an inversion to a new circle  $C'$  with radius  $r'$  and center  $\mathbf{m}'$  with

$$r' = \frac{r}{|\mathbf{m}^2 - r^2|} \quad \text{and} \quad \mathbf{m}' = \frac{\mathbf{m}}{\mathbf{m}^2 - r^2} \quad . \quad (12)$$

The shaded circles shown in Figure 3a obey  $\mathbf{m}^2 - r^2 = 1$  which leads to the inversion symmetry of the displayed structure.

Figure 3b shows cross-sections which are generated by inversions centered at points along different lines of symmetry. They consist of three different circles and approximate the cross-section of Willmore surfaces with the  $X$ - $Y$ -plane. As the inversion center  $\mathbf{a}$ , starting with  $\mathbf{a} = (0, 0, 0)$ , is moved along one of the symmetry lines, the threefold symmetry is broken but one symmetry plane (in addition to the  $X$ - $Y$ -plane) is conserved. Three different types of  $C_{2v}$ -symmetric Willmore surfaces can be generated, see Figures 3b and 4: Surfaces of the type  $C_{LS}$  begin with the Lawson surface  $L$  and end with a limit shape  $S$ . The shapes  $C_{BL}$  connect

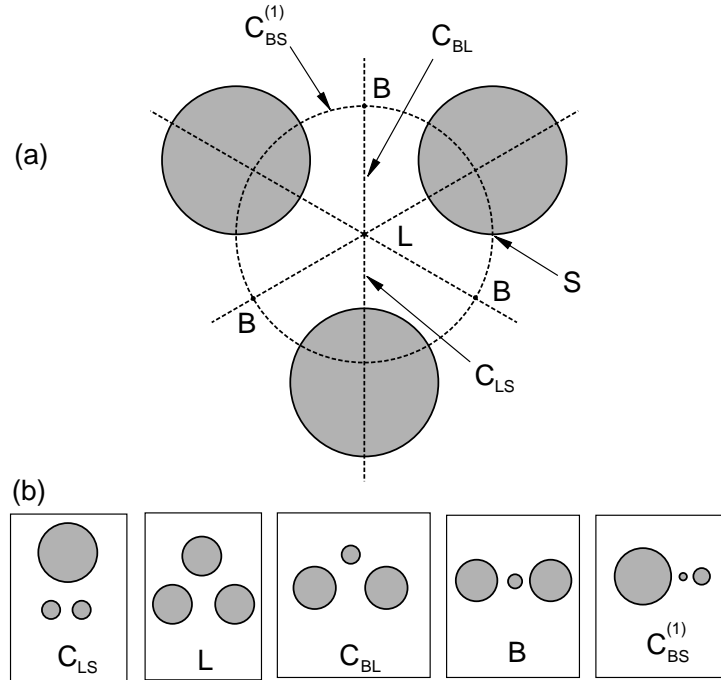


Fig. 3. — (a) Two-dimensional model geometry used to discuss the action of conformal transformations applied to the Lawson surface. The shaded circles represent the cross-sections of  $L$  with the  $X$ - $Y$ -plane. Inversions centered at points along the broken lines generate the families  $C_{LS}$ ,  $C_{BL}$  and  $C_{BS}^{(1)}$  of Willmore surfaces. The point  $B$  corresponds to the button surface. For details see text. (b) Configurations generated by inversions centered along the lines  $C_{LS}$ ,  $C_{BL}$  and  $C_{BS}^{(1)}$  as indicated in (a). They represent cross-sections of Willmore surfaces with the  $X$ - $Y$ -plane.

the Lawson surface with the button surface  $B$ . A third family  $C_{BS}^{(1)}$  of  $C_{2v}$ -symmetric surfaces connects the button surface with limit shapes  $S$ .

The button surface is shown in Figure 5. It is generated by an inversion which is centered at the intersection of the mirror planes of the Lawson surface with its sphere of inversion symmetry, see Figure 3b. The button surface and the Lawson surface are the only Willmore surfaces of  $\mathcal{W}_2$  which have three mirror planes that intersect in a point.

The families of Willmore surfaces described so far are mirror symmetric with respect to the  $X$ - $Y$ -plane. This mirror symmetry is broken as soon as  $a_Z \neq 0$ . Two new families of Willmore surfaces with at least two mirror planes can be generated by inversions with  $a_Z \neq 0$ : (i) a family  $C_{LS}^{(1)}$  of  $C_{3v}$ -symmetric shapes which connects the Lawson surface  $L$  with limit shapes  $S$ . The corresponding centers of inversion  $\mathbf{a} = (0, 0, a_Z)$  are located on the  $Z$ -axis. And (ii) a family  $C_{BS}^{(1)}$  of  $C_{2v}$ -symmetric shapes which connects the button surface  $B$  with limit shapes  $S$ . The centers of inversion in this case are given by the circular arc defined by the cross-section of the  $Y$ - $Z$ -plane with the sphere of inversion symmetry of  $L$ . The shapes shown in Figure 4 represent each of the families of Willmore surfaces introduced above. These shapes were generated by applying SCT's on the Lawson surface  $L$ .

4.4. CLASSIFICATION OF WILLMORE SURFACES. — The complete structure and topology of  $\mathcal{W}_2$  can now be summarized as follows: The “boundary” of  $\mathcal{W}_2$  is given by inversion centers

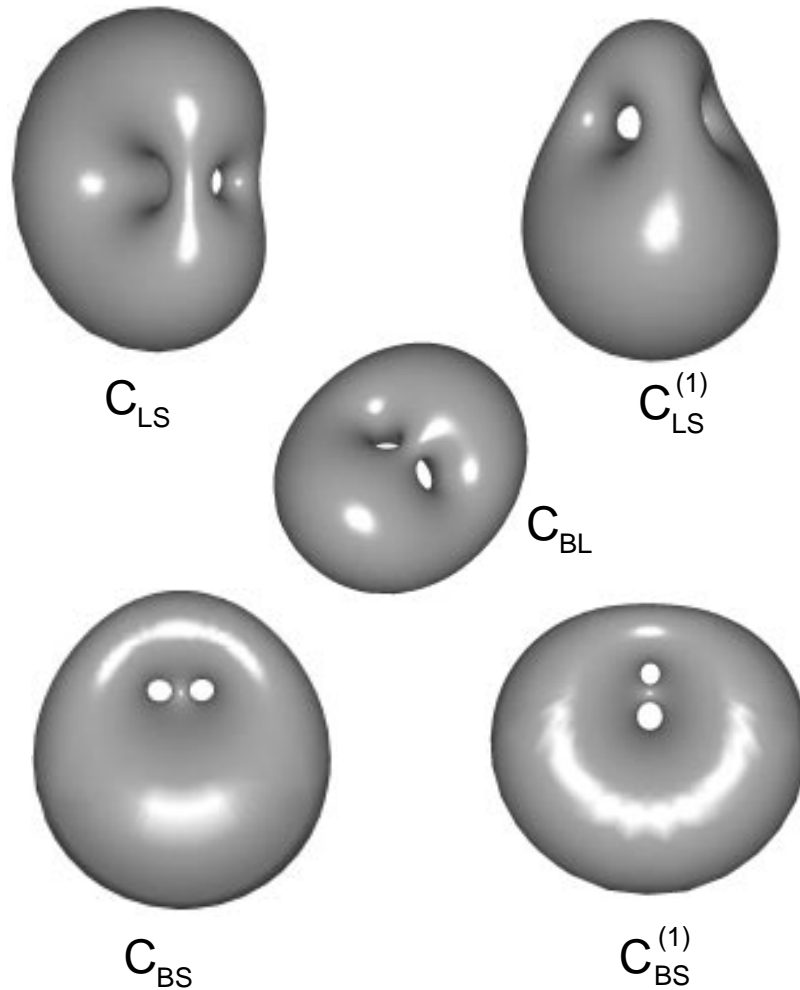


Fig. 4. — Shapes which represent different families of Willmore surfaces. The shapes  $C_{LS}$ ,  $C_{BL}$ ,  $C_{BS}$  and  $C_{BS}^{(1)}$  have  $C_{2v}$ -symmetry, the shapes  $C_{LS}^{(1)}$  are  $C_{3v}$ -symmetric.

**a** located on the original Lawson surface. Corresponding Willmore surfaces are singular limit shapes  $S$ . The interior of  $L$  corresponds to the three-dimensional set of nonsingular Willmore surfaces. Inversion centers **a** located on a symmetry surface of  $L$  correspond to Willmore surfaces with at least one mirror plane ( $C_{1v}$ -symmetry). Those shapes form a two dimensional subspace of  $\mathcal{W}_2$ . Lines of intersection of two symmetry surfaces correspond to one-dimensional families of Willmore surfaces. These surfaces have at least two symmetry planes ( $C_{2v}$  and  $C_{3v}$ -symmetry) and are all displayed in Figure 4. Willmore surfaces of highest symmetry are found at distinct points where three symmetry surfaces intersect in a point: The  $\mathcal{D}_{2h}$ -symmetric button surface and the  $\mathcal{D}_{3h}$ -symmetric Lawson surface.

4.5. HIGHER TOPOLOGICAL GENUS. — These arguments can be extended to Lawson surfaces of higher topological genus  $g$ . Lawson surfaces for  $g > 2$  again have a sphere of inversion symmetry and  $\mathcal{D}_{gh}$  symmetry [29,33]: In addition to the  $X$ - $Y$  mirror plane they have a  $(g + 1)$ -

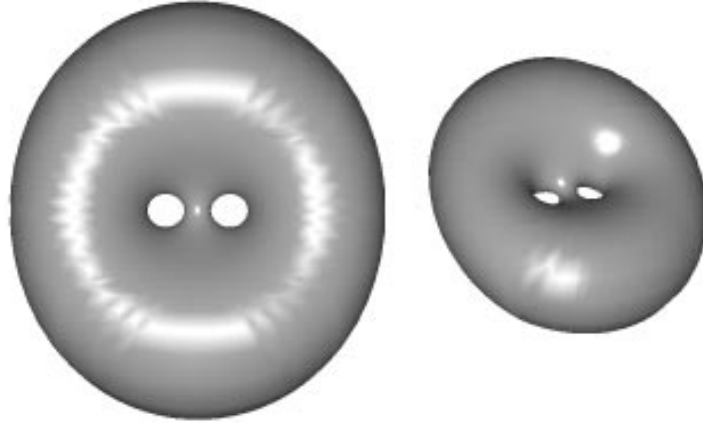


Fig. 5. — Two views of the  $\mathcal{D}_{2h}$ -symmetric button surface  $B$  with topological genus  $g = 2$ .

fold symmetry and  $(g + 1)$  mirror planes which contain this axis. All symmetry arguments given here for  $g = 2$  can be generalized and corresponding families of Willmore surfaces can be defined. Note that these arguments which use the symmetry properties of the minimal surfaces  $\xi_{1g}$  are based on the assumption that Kusner's conjecture [30] is valid.

## 5. Willmore Surfaces as Vesicle Shapes

In general, a vesicle shape is calculated in the BC-model by minimizing the bending energy for fixed values of the reduced volume  $v$  and the reduced total mean curvature  $m$ . A Willmore surface parameterized by the vector  $\mathbf{a}$  has a well defined reduced volume  $v(\mathbf{a})$  and reduced total mean curvature  $m(\mathbf{a})$ . Since it is an absolute minimum of  $G$  it is a special solution to the vesicle shape problem for a point with  $v = v(\mathbf{a})$  and  $m = m(\mathbf{a})$  in the  $(v, m)$ -plane of the phase diagram of the BC-model. This mapping  $\mathbf{a} \rightarrow (v(\mathbf{a}), m(\mathbf{a}))$  defines a region  $W$  in the  $(v, m)$ -plane where Willmore surfaces occur as solutions of the BC-model.

5.1. WILLMORE SURFACES IN THE  $(v, m)$ -PLANE. — The region  $W$  of Willmore surfaces in the  $(v, m)$ -plane can be studied looking at infinitesimal conformal transformations  $\mathbf{a}' = \mathbf{a} + \delta\mathbf{a}$  with  $|\delta\mathbf{a}| \ll 1$ . An initial Willmore surface with  $v = v(\mathbf{a})$  and  $m = m(\mathbf{a})$  is deformed to a new surface with reduced volume  $v' = v + \delta v$  and reduced total mean curvature  $m' = m + \delta m$ . To linear order in  $\delta\mathbf{a}$ , this transformation can be expressed as [24]

$$\delta v = v \mathbf{A}^{(v)} \cdot \delta\mathbf{a} + O(\delta\mathbf{a}^2) \quad (13)$$

$$\delta m = m \mathbf{A}^{(m)} \cdot \delta\mathbf{a} + O(\delta\mathbf{a}^2) \quad (14)$$

The vector coefficients

$$\begin{aligned} \mathbf{A}^{(v)} &\equiv 6(\mathbf{R}^A - \mathbf{R}^V) \\ \mathbf{A}^{(m)} &\equiv 2(\mathbf{R}^A - \mathbf{R}^M) \end{aligned} \quad (15)$$

are related to the center of area  $\mathbf{R}^A$ , the center of volume  $\mathbf{R}^V$  and the center of mean curvature

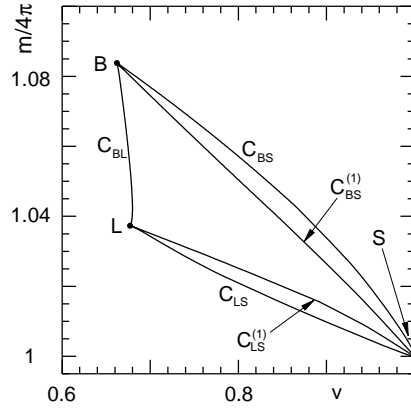


Fig. 6. — Reduced volume  $v$  and reduced total mean curvature  $m$  of the families  $C_{BL}$ ,  $C_{LS}$ ,  $C_{LS}^{(1)}$ ,  $C_{BS}$  and  $C_{BS}^{(1)}$  of Willmore surfaces. The Lawson surface  $L$ , the Button-surface  $B$  and limit shapes  $S$  are located at distinct points.

$\mathbf{R}^M$ , of the Willmore surface characterized by  $\mathbf{a}$ . These centers are defined as

$$\begin{aligned}
 \mathbf{R}^A &\equiv \frac{1}{A} \oint dA \mathbf{R} \\
 \mathbf{R}^V &\equiv \frac{1}{V} \int dV \mathbf{R} \\
 \mathbf{R}^M &\equiv \frac{1}{M} \oint dA H \mathbf{R} \quad .
 \end{aligned}
 \tag{16}$$

The centers of area, volume and mean curvature are located within all symmetry planes of a given surface. The effects of infinitesimal conformal transformations are therefore closely linked to the symmetry properties of a surface. For a surface with less than two symmetry planes (less than  $C_{2v}$ -symmetry) the points  $\mathbf{R}^A$ ,  $\mathbf{R}^V$  and  $\mathbf{R}^M$  define a plane which is spanned by the vectors  $\mathbf{A}^{(v)}$  and  $\mathbf{A}^{(m)}$ .  $\mathbf{A}^{(v)}$  and  $\mathbf{A}^{(m)}$  are linearly independent in this case. If a surface is  $C_{2v}$ -symmetric, the points  $\mathbf{R}^A$ ,  $\mathbf{R}^V$  and  $\mathbf{R}^M$  fall on a straight line which is the intersection of two mirror planes. The vectors  $\mathbf{A}^{(v)}$  and  $\mathbf{A}^{(m)}$  are collinear and point along this line. If a surface has a center of symmetry where more than two mirror planes intersect in a point,  $\mathbf{A}^{(v)} = \mathbf{A}^{(m)} = \mathbf{0}$ . This is the case for the Lawson surface  $L$  and the button surface  $B$ .

The effect of infinitesimal conformal transformations differs in these cases. If  $\delta\mathbf{a}$  covers the interior of an infinitesimal sphere, this sphere is mapped onto a small region surrounding the point  $(v(\mathbf{a}), m(\mathbf{a}))$  if  $\mathbf{A}^{(v)}$  and  $\mathbf{A}^{(m)}$  are linearly independent. If, on the other hand,  $\mathbf{A}^{(v)}$  and  $\mathbf{A}^{(m)}$  are collinear, a sphere is mapped onto a line segments in the  $(v, m)$ -plane. In the case of the Lawson surface and the button surface with  $\mathbf{A}^{(v)} = \mathbf{A}^{(m)} = \mathbf{0}$ , an infinitesimal sphere is mapped onto the point  $(v(\mathbf{a}), m(\mathbf{a}))$ . It follows from this observation that shapes with less than  $C_{2v}$  symmetry correspond to points which are located in the interior of the region  $W$  and that the boundaries of  $W$  in the  $(v, m)$ -plane correspond to shapes with  $C_{2v}$ ,  $D_{2h}$  and  $D_{3h}$  symmetry.

In order to determine the shape and the location of  $W$  in the phase diagram, it is sufficient to locate the families of shapes with  $C_{2v}$ ,  $D_{2h}$  and  $D_{3h}$  symmetry in the  $(v, m)$ -plane. Figure 6 displays lines which correspond to these families of Willmore surfaces. The boundary of  $W$  is given by the utmost of these lines and corresponds to the shapes  $C_{BL}$ ,  $C_{LS}$  and  $C_{BS}$ .

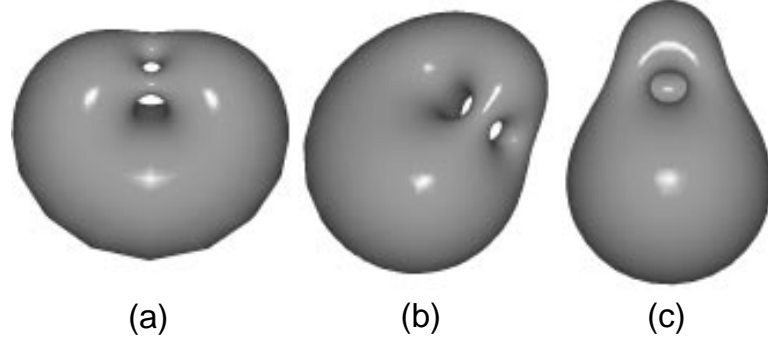


Fig. 7. — Three examples of shapes along the conformal mode with reduced volume  $v = 0.78$  and  $m = 1.027 \cdot 4\pi$ . The shapes (a) and (c) are  $C_{1v}$ -symmetric while shape (b) has no symmetries.

The Lawson surface  $L$  with  $(v, m) \simeq (0.67, 1.037 \cdot 4\pi)$ , the button surface  $B$  with  $(v, m) \simeq (0.66, 1.084 \cdot 4\pi)$  and the spherical limit shapes  $S(v, m) \simeq (1, 4\pi)$  form vertices of the region  $W$ . The shapes  $C_{LS}^{(1)}$  and  $C_{BS}^{(1)}$  together with Willmore surfaces with less than two mirror planes are located in the interior of  $W$ .

## 6. Conformal Degeneracy and Conformal Diffusion

If the three-dimensional set  $\mathcal{W}_2$  of Willmore surfaces is mapped onto the  $(v, m)$ -plane, a one-dimensional subset  $\mathcal{W}_2(v, m)$  of shapes is mapped on a single point  $(v, m)$ . The vesicle shape for these values of  $v$  and  $m$  is therefore not uniquely defined and the ground state is degenerate. The one-dimensional set  $\mathcal{W}_2(v, m)$  of degenerate ground states is called a conformal mode. Figure 7 shows as an example three different shapes with  $v = 0.78$  and  $m = 1.027 \cdot 4\pi$  which are conformally equivalent and which are minima of the energy  $G$ . The existence of conformal modes for topological genus  $g > 2$  is a direct consequence of conformal invariance. Two physical constraints are not sufficient to remove the degeneracy of the Willmore problem and a one-dimensional degeneracy remains.

6.1. CONFORMAL MODES. — Conformal modes are families of Willmore surfaces which can be parameterized by a curve  $\mathbf{a}(s)$ . This curve contains those vectors  $\mathbf{a}$  which correspond to Willmore surfaces with the same values of  $v$  and  $m$ . Therefore, a conformal mode obeys

$$\frac{dv(\mathbf{a}(s))}{ds} = \frac{dm(\mathbf{a}(s))}{ds} = 0 \quad , \quad (17)$$

or

$$\frac{d\mathbf{a}}{ds} \cdot \mathbf{A}^{(v)} = \frac{d\mathbf{a}}{ds} \cdot \mathbf{A}^{(m)} = 0 \quad . \quad (18)$$

A conformal mode therefore satisfies the differential equation [27]

$$\frac{d\mathbf{a}}{ds} = \frac{\mathbf{A}^{(v)} \times \mathbf{A}^{(m)}}{|\mathbf{A}^{(v)} \times \mathbf{A}^{(m)}|} \quad , \quad (19)$$

where  $s$  is chosen to be the arclength of  $\mathbf{a}(s)$  with  $|d\mathbf{a}/ds| = 1$ .

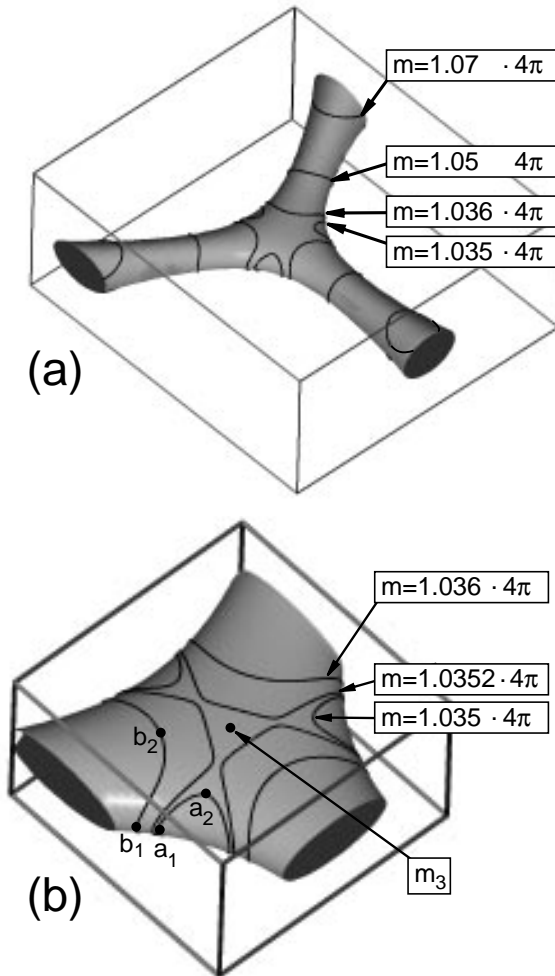


Fig. 8. — (a) Surface  $S_v$  which represents the set of Willmore surfaces with reduced volume  $v = 0.7$ . The lines on  $S_v$  indicate conformal modes for different values of the reduced total mean curvature  $m$ . (b) Detailed plot of the surface shown in (a) close to  $m = m_3 \simeq 1.0351 \cdot 4\pi$  to demonstrate the topology change of conformal modes at  $m = m_2 \simeq 1.0352 \cdot 4\pi$  and  $m = m_3$ . The points  $a_1, a_2, b_1$  and  $b_2$  correspond to the Willmore surfaces shown in Figure 9.

6.2. STRUCTURE AND TOPOLOGY OF CONFORMAL MODES. — A conformal mode can be described as the intersection  $S_v \cap S_m$  of two surfaces  $S_v$  and  $S_m$ . Here,  $S_v$  is the surface defined by those points  $\mathbf{a}$  which correspond to Willmore surfaces with given reduced volume  $v$ . Similarly,  $S_m$  represents those points which correspond to Willmore surfaces with given total mean curvature  $m$ . The surface  $S_v$  is displayed in Figure 8 for  $v = 0.7$ . It has the symmetry and the topology of the Lawson surface. Conformal modes are curves on this surface. Some examples of conformal modes for  $v = 0.7$  are shown in Figures 8a and b for different values of  $m$ . They have been obtained by numerical integration of equation (19).

Conformal modes are always closed curves: A conformal mode cannot end and it cannot diverge to infinity [40]. Therefore, conformal modes can be classified by their topology with

respect to the surface  $S_v$ . Two different types of conformal modes can be distinguished: (i) conformal modes which can be contracted to a point on  $S_v$  and (ii) conformal modes which cannot be contracted. Two examples for the first case are the conformal modes with  $(v, m) = (0.7, 1.035 \cdot 4\pi)$  and  $(v, m) = (0.7, 1.07 \cdot 4\pi)$ , see Figure 8. Conformal modes of this type exist in the neighborhood of the boundary lines  $C_{BS}$  and  $C_{LS}$  of  $W$ . As one of these boundary lines is reached, the conformal modes contract to a point on  $S_v$ . This point corresponds to a shape  $C_{LS}$  or  $C_{BS}$ , respectively, for which no degeneracy occurs.

An example for the second type of conformal modes is given by the point  $(v, m) = (0.7, 1.05 \cdot 4\pi)$ . Moving from this point to one of the boundary lines of  $W$ , the topology of the conformal mode on the surface  $S_v$  changes. This topology change occurs along two lines  $m = m_1(v)$  and  $m = m_2(v)$  in the  $(v, m)$ -plane. For  $v = 0.7$ ,  $m_1 \simeq 1.0745 \cdot 4\pi$  and  $m_2 \simeq 1.0352 \cdot 4\pi$ .

The line  $m_1(v)$  corresponds to the shapes  $C_{BS}^{(1)}$ . Along the line  $m = m_2$ , the situation is more difficult. At  $m = m_2(v)$ , a conformal mode divides into two distinct closed curves which can both be contracted to a point. An example for this situation is shown in Figure 8b. One of the two closed curves vanishes for  $m = m_3(v) < m_2(v)$  in a single point. Here, the line  $m_3(v)$  corresponds to the shapes  $C_{LS}^{(1)}$ . The difference between  $m_2(v)$  and  $m_3(v)$  is small. For  $v = 0.7$ ,  $m_2 - m_3 \simeq 10^{-4}$ .

Figures 9a and b show two pairs of  $\mathcal{C}_{1v}$ -symmetric shapes along the conformal modes with  $m \simeq 1.035 \cdot 4\pi < m_2$  and  $m \simeq 1.036 \cdot 4\pi > m_2$ , respectively. The location of these shapes on  $S_v$  is indicated in Figure 8b. These conformal modes have different topology with respect to the surface  $S_v$ . Consequently, the shape  $a_2$  differs qualitatively from  $b_2$  while  $a_1$  and  $b_1$  are not distinguishable.

The topology change of conformal modes corresponds to a discontinuous change of the structure of these modes. This discontinuity does not correspond to a phase transition in the phase diagram since it does not lead to a non-analytic behavior of the energy  $G(v, m)$ .

**6.3. CONFORMAL DIFFUSION.** — The existence of conformal modes affects the behavior of vesicles of topological genus  $g \geq 2$ . If such a vesicle is prepared within the region  $W$  of the phase diagram, the conformal degeneracy leads to shape fluctuations called conformal diffusion.

The difference between bending modes of regular vesicles and conformal diffusion can be described as follows. Bending modes are thermal excitations which are governed by the bending rigidity of the membrane. If the ground-state of a vesicle is unique, the shape which minimizes the energy for given  $v$  and  $m$  is a surface  $\mathbf{R}_0(s^1, s^2)$  which can be parameterized by two coordinates  $s^1, s^2$ . Small deformations of this shape can be expanded as

$$\mathbf{R}(s^1, s^2) = \mathbf{R}_0(s^1, s^2) + \mathbf{n}(s^1, s^2) \sum_{i=0}^{\infty} a_i f_i(s^1, s^2) \quad , \quad (20)$$

where  $\mathbf{n}$  denotes the normal on the surface and the  $a_i$  denotes the amplitude of the  $i$ -th mode. The functions  $f_i(s^1, s^2)$  are normalized eigenfunctions of the second variation  $\delta^2 G|_{(v,m)}$  of the bending energy for fixed  $v$  and  $m$ . The eigenvalues are denoted  $g_i$ . The energy of a deformed shape then reads

$$G = G_0 + \frac{1}{2} \sum_{i=0}^{\infty} g_i a_i^2 + O(a_i^3) \quad , \quad (21)$$

where  $G_0$  is the bending energy of the shape  $\mathbf{R}_0$ . For small deformations or small temperature  $T < \kappa$ , terms of higher order in  $a_i$  can be neglected. The eigenmodes decouple and the amplitudes of the bending modes obey

$$\langle a_i^2 \rangle = \frac{T}{g_i} \quad . \quad (22)$$

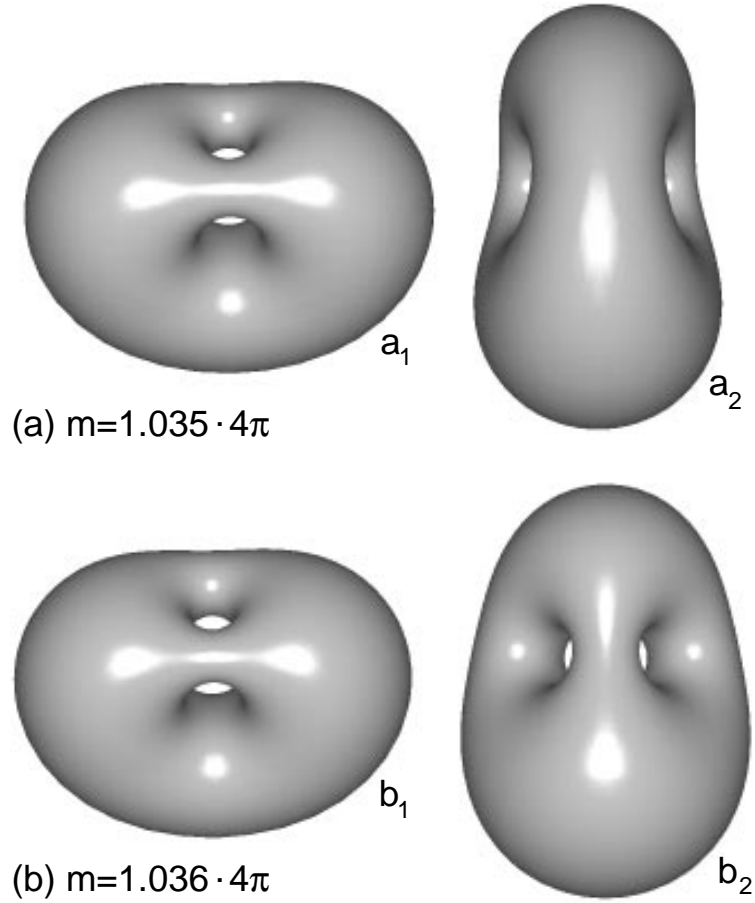


Fig. 9. — (a) Two Willmore surfaces with  $(v, m) = (0.7, 1.035 \cdot 4\pi)$  which are part of a conformal mode. Both shapes have one symmetry plane. (b) The corresponding shapes with  $(v, m) = (0.7, 1.036 \cdot 4\pi)$ . The position of these shapes on the surface  $S_v$  is indicated in Figure 8.

Here, the brackets denote the thermal expectation value. The eigenmode  $i$  relaxes within a typical relaxation time

$$t_b^{(i)} = \frac{1}{\gamma_i g_i} \quad , \quad (23)$$

where  $\gamma_i$  is a coefficient of viscous damping. Dimensional arguments suggest that  $\gamma_0 \sim 1/(\eta R_0^3)$ , where  $R_0$  is the vesicle size and  $\eta$  denotes the viscosity of the solvent. The longest relaxation time of bending modes therefore obeys [41]

$$t_b \sim \frac{\eta R_0^3}{\kappa} \quad . \quad (24)$$

A different situation occurs, if the ground-state is conformally degenerate. In this case, a shape  $\mathbf{R}_0$  with  $s = s_0$  can be selected along a conformal mode  $\mathbf{a}(s)$ . The conformal mode is eigenmode  $f_0(s^1, s^2)$  with  $g_0 = 0$ . In addition, all higher variations of the energy vanish in this case. If this mode is thermally excited, the shape performs a diffusive motion in shape space.

This conformal diffusion can be approximately described by assuming that  $ds$  is the correct measure in shape space. In this approximation,

$$\langle s^2 \rangle \approx D_{\text{cf}} t \quad , \quad (25)$$

where  $D_{\text{cf}} \sim T/(\eta R_0)$  is a diffusion constant. The typical time-scale of conformal diffusion is given by [26]

$$t_{\text{cf}} \sim \frac{\eta R_0^3}{T} \quad . \quad (26)$$

For phospholipid membranes  $\kappa/T \simeq 25$  [42–44]. Shape fluctuations which correspond to conformal diffusion occur on time-scales which are long compared to bending modes since  $t_{\text{cf}} \gg t_{\text{b}}$ .

Conformal diffusion is closely related to translational and rotational diffusion. In fact, translations and rotations form a subgroup of conformal transformations. Therefore, translational and rotational diffusion are special cases of conformal diffusion and the typical time-scale which corresponds to these diffusion processes is of the same order of magnitude as  $t_{\text{cf}}$ .

## 7. Phase Diagrams and Shape Transformations

Within a certain region  $W$  in the phase diagram of the BC-model vesicle shapes are given by Willmore surfaces with  $G = G_2$ . These shapes in general have no mirror symmetries. Shapes of minimal energy which correspond to points  $(v, m)$  located outside the region  $W$  are not given by Willmore surfaces. The bending energy of these shapes obeys  $G(v, m) > G_2$ . In principle, these shapes have to be determined by minimization of  $G$  for given constraints. In the following subsections, it is shown that the topology of the phase diagram is already determined by the structure of the region  $W$ . The symmetry of vesicle shapes outside  $W$  can be obtained from the symmetry of Willmore surfaces at the boundary of  $W$ . This fact follows from the lever rule which is a consequence of the conformal invariance of  $G$ . Furthermore, the lever rule shows that conformal modes can only exist within the region  $W$  and that shapes outside  $W$  are unique.

**7.1. THE LEVER RULE.** — The lever rule can be derived as follows. Infinitesimal SCT's as given by equation (9) with  $|\mathbf{a}| \ll 1$  are applied to a shape of minimal energy  $G(v, m)$  with reduced volume  $v$  and reduced total mean curvature  $m$ . This transformation generates a new shape with unchanged energy  $G' = G(v, m)$ . It has reduced volume  $v' = v + \delta v$  and reduced total mean curvature  $m' = m + \delta m$  with [24]

$$\delta v = v \mathbf{A}^{(v)} \cdot \mathbf{a} + O(\mathbf{a}^2) \quad , \quad (27)$$

$$\delta m = m \mathbf{A}^{(m)} \cdot \mathbf{a} + O(\mathbf{a}^2) \quad . \quad (28)$$

Here,  $\mathbf{A}^{(v)}$  and  $\mathbf{A}^{(m)}$  are again given by equation (15). The new shape is compared to the shape with energy  $G(v', m')$  at the point  $(v', m')$ . Since  $G(v', m')$  is the energy minimum,

$$G(v', m') \leq G' \quad . \quad (29)$$

Expanding  $G(v, m)$  at  $(v, m)$ , the energy  $G(v', m')$  can be expressed as

$$G(v', m') = G(v, m) + \left( v \frac{\partial G}{\partial v} \mathbf{A}^{(v)} + m \frac{\partial G}{\partial m} \mathbf{A}^{(m)} \right) \cdot \mathbf{a} + O(\mathbf{a}^2) \quad . \quad (30)$$

The condition (29) can only be valid for arbitrary  $\mathbf{a}$  if

$$v \frac{\partial G}{\partial v} \mathbf{A}^{(v)} + m \frac{\partial G}{\partial m} \mathbf{A}^{(m)} = 0 \quad . \quad (31)$$

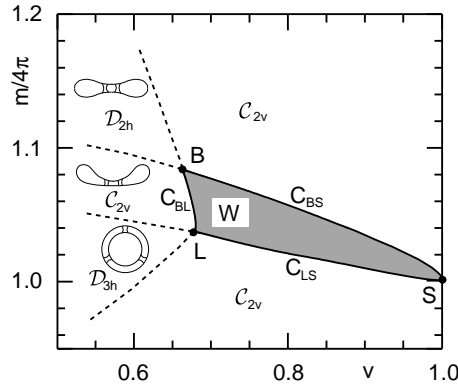


Fig. 10. — Phase diagram for vesicles of topological genus  $g = 2$  in the BC-model. Within the region  $W$ , which is bounded by the lines  $C_{BS}$ ,  $C_{BL}$  and  $C_{LS}$ , the ground state is conformally degenerate and shapes are given by Willmore surfaces. The Lawson surface  $L$ , the button surface  $B$  and limit shapes  $S$  occur at the vertices of  $W$ . Five additional regions exist in the phase diagram. The symmetries of shapes within these regions are indicated. Three families of shapes are indicated schematically.

Equation (31) is the so-called lever rule which must be obeyed by any shape of minimal energy [24]. The lever rule is trivial within the region  $W$  where  $\partial G/\partial v = \partial G/\partial m = 0$ . Outside of  $W$ ,  $\partial G/\partial v \neq 0$  and  $\partial G/\partial m \neq 0$ . Therefore,  $\mathbf{A}^{(v)}$  and  $\mathbf{A}^{(m)}$  obey

$$\mathbf{A}^{(v)} = \lambda \mathbf{A}^{(m)} \quad , \quad (32)$$

where  $\lambda$  is a real number. The vectors  $\mathbf{A}^{(v)}$  and  $\mathbf{A}^{(m)}$  are collinear by symmetry if a given shape has at least two planes of reflection symmetry or at least  $C_{2v}$ -symmetry [45]. The value of  $\lambda$  is then determined by equation (31). For shapes with three symmetry-planes which intersect in a point,  $\mathbf{A}^{(v)} = \mathbf{A}^{(m)} = \mathbf{0}$ , and the lever rule is satisfied by the symmetry properties of the shape alone.

A consequence of the lever rule is that conformal modes cannot exist outside the region  $W$ . Since  $\mathbf{A}^{(m)}$  and  $\mathbf{A}^{(v)}$  are collinear, no solution to equation (19) exists. As a result, energy minima are unique.

The existence of unique energy minima follows from the collinearity of  $\mathbf{A}^{(m)}$  and  $\mathbf{A}^{(v)}$ . As described in Section 6.2, conformal modes vanish as the boundary of  $W$  is reached. At the same time, Willmore surfaces become symmetric and  $\mathbf{A}^{(v)}$  and  $\mathbf{A}^{(m)}$  become collinear by symmetry. Since the collinearity of  $\mathbf{A}^{(v)}$  and  $\mathbf{A}^{(m)}$  persists at the exterior of  $W$ , the corresponding shapes adopt the symmetries of Willmore surfaces along the boundary of  $W$ .

7.2. PHASE DIAGRAM OF THE BC-MODEL. — The phase diagram for genus-2 vesicles in the BC-model is shown in Figure 10. It contains the region  $W$  of Willmore surfaces. Within this region, shapes in general are asymmetric and conformal modes exist. Five additional regions occur where shapes are symmetric and unique: (i) A region of  $D_{2h}$ -symmetric genus-2 discocytes, (ii) a region of  $D_{3h}$ -symmetric shapes, (iii) a region of  $C_{2v}$ -symmetric genus-2 stomatocytes and (iv) and (v) two regions containing  $C_{2v}$ -symmetric shapes. The lines  $C_{LS}$ ,  $C_{BL}$  and  $C_{BS}$  separate the region  $W$  from the regions of  $C_{2v}$ -symmetric shapes. The two remaining regions obtain their symmetries from the button- and the Lawson surface.

Along the boundaries of the region  $W$ , the symmetries of shapes are broken continuously by conformal transformations. These boundary lines therefore represent continuous shape

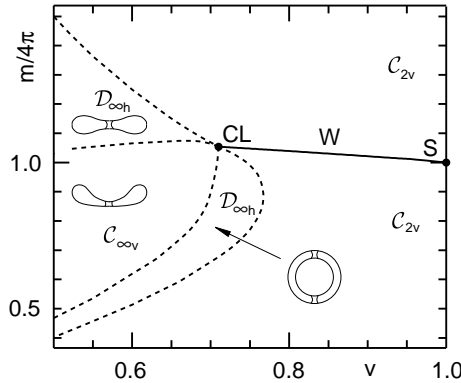


Fig. 11. — Phase diagram for vesicles of toroidal topology in the BC-model for comparison with Figure 10. Willmore surfaces of topological genus  $g = 1$  exist along the line  $W$  which connects the Clifford torus  $CL$  with a limit shape  $S$ . The axisymmetric families of shapes are indicated schematically.

transformation lines. Additional shape transformation lines exist between regions with shapes of different symmetries. They are indicated by broken lines in Figure 10. The exact locations of these lines in the phase diagram are not known.

This phase diagram can be compared to the phase diagram of toroidal vesicles as shown in Figure 11 which has been determined elsewhere [26]. For toroidal topology or  $g = 1$ , Willmore surfaces fall on a line  $W$  which connects the Clifford Torus  $CL$  and a limit shape  $S$ . This line does not correspond to a phase boundary since Willmore surfaces along this line have the same symmetry as shapes above and below this line. Furthermore, no conformal modes exist for  $g = 1$  and vesicle shapes are always unique. Three regions of axisymmetric shapes occur in the phase diagram for toroidal topology: (i)  $\mathcal{D}_{\infty h}$ -symmetric discoid tori, (ii)  $\mathcal{C}_{\infty v}$ -symmetric toroidal stomatocytes and (iii)  $\mathcal{D}_{\infty h}$ -symmetric sickle-shaped tori. These regions of axisymmetric shapes correspond to the regions of genus-2 discocytes, genus-2 stomatocytes and  $\mathcal{D}_{3h}$ -symmetric shapes.

The phase diagrams for  $g = 1$  and  $g = 2$  have similar topology. The main difference is the location of Willmore surfaces which is a line for  $g = 1$  and a region for  $g = 2$ . Note that the topology of the  $g = 2$  phase-diagram can be determined from the properties of Willmore surfaces alone, while for  $g = 1$  the knowledge of Willmore surfaces is not sufficient [26].

The arguments given here to obtain the phase diagram for topological genus  $g = 2$  extend to higher topological genus  $g > 2$ . The Willmore surfaces of lowest energy  $G = G_g$  are Lawson-surfaces of topological genus  $g$ . This surface together with conformal transformations again leads to a region  $W$  with conformally degenerate ground state. Adjacent to  $W$ , vesicle shapes are unique and they adopt the symmetries of Willmore surfaces along the boundaries of  $W$ . For  $g > 2$  additional regions with degenerate ground states could occur. For  $g = 3$ , there is evidence for the existence of a Willmore surface which is a local minimum of  $G$  with  $G > G_3$  [29]. This surface has tetrahedral symmetry and corresponds to a minimal surface in  $S^3$  discovered by Karcher, Pinkall and Sterling called  $\tau$ -surface [34]. This surface together with its conformal transformations corresponds to locally stable energy minima in the BC-model. If it corresponds to an absolute energy minimum for the given physical constraints, a second region  $W'$  with conformally degenerate ground-state would exist in the phase diagram for  $g = 3$ .

7.3. CONFORMAL DEGENERACY IN THE ADE-MODEL. — The existence of conformal degeneracy of the ground state in the BC-model is a consequence of two constraints imposed in this model. In the ADE-model introduced in Section 2.2, one of these constraints is replaced by an additional term which contributes to the elastic energy. The existence of conformal degeneracy in the ADE-model can be shown as follows. In the ADE-model, the relevant parameters are the reduced volume  $v$  and the relaxed mean curvature  $m_0$ . The energy  $W(v, m_0)$  can be obtained from the energy  $G(v, m)$  by the transformation [13]

$$W(v, m_0) = G(v, m[m_0]) + \frac{\kappa\alpha}{2}(m[m_0] - m_0)^2 \quad , \quad (33)$$

where the function  $m[m_0]$  is implicitly given by

$$\frac{\partial G}{\partial m} = -\kappa\alpha(m - m_0) \quad . \quad (34)$$

This transformation simplifies if it is applied to Willmore surfaces. Within the region  $W$ ,  $\partial G/\partial m = 0$ , and  $m[m_0] = m_0$ . The region  $W$  in the  $(v, m)$ -plane is therefore mapped to an identical region  $\tilde{W}$  in the  $(v, m_0)$ -plane. At a given point  $(v, m_0)$  within this region, there exists a conformal mode which is identical to the conformal mode  $(v, m = m_0)$  in the BC-model. This argument does not depend on the value of the parameter  $\alpha$ . The results on conformal degeneracy of the previous sections apply also to the ADE-model.

The location of phase boundaries in the phase diagram which are not given by boundary lines of  $W$  does depend on the value of  $\alpha$ . Furthermore, additional shape transformation lines occur in the ADE-model for small values of  $\alpha$ . Beginning with the BC-model which corresponds to  $\alpha = \infty$ , these lines occur as soon as  $\partial^2 G/\partial m^2 = -\kappa\alpha$  is satisfied at a point along the boundary of  $W$  [13].

## 8. Discussion

The morphology of vesicles of spherical topology is hardly affected by the conformal invariance of the bending energy of the membrane. This invariance, however, has dramatic consequences for the morphology of vesicles of topological genus  $g > 1$ . The aim of this paper is to demonstrate this effect for the case  $g = 2$  and to study the relation between Willmore surfaces and vesicle shapes.

Willmore surfaces are defined as solutions to the Willmore problem which is a purely mathematical problem [20]. They are stereo-graphic images of minimal surfaces  $\xi_{1g}$  in  $S^3$  as conjectured by Kusner [30, 33]. The symmetries and the properties of the minimal surfaces  $\xi_{1g}$  completely determine the morphology of vesicles of higher topological genus. As a result, the conformal invariance of the bending energy leads to a degeneracy of vesicle shapes in the phase diagram of curvature models. The soft mode which corresponds to this degeneracy is given by conformal transformations. Vesicles with conformally degenerate ground state exhibit conformal diffusion where conformal transformations become observable under the microscope [19].

Vesicles of topological genus  $g = 2$ ,  $g = 3$ , and vesicles of higher genus have been observed experimentally by Michalet and Bensimon [18, 19]. For  $g = 2$ , shapes with different symmetries were observed: Genus-2 discocytes similar to the button surface, Genus-2 stomatocytes and  $\mathcal{D}_{3h}$ -symmetric shapes close to the Lawson-surface. Furthermore, stable shapes with  $\mathcal{C}_{2v}$ -symmetry were found. All symmetries observed are in agreement with the phase diagram shown in Figure 10 [18, 19].

In addition, genus-2 vesicles were observed which seemed to have no symmetry planes. It was demonstrated that these vesicles exhibited pronounced shape changes on a time scale of

$\sim 30$  s. The behavior of these vesicles appeared different from those with symmetry planes. Michalet and Bensimon concluded that these vesicles are examples for conformal diffusion [19].

The experimental observations of Michalet and Bensimon confirm the theoretical results described in this paper and strongly support the validity of curvature models for the description of vesicle shapes. Furthermore, these observations demonstrate that the energy of fluid membranes is indeed a conformal invariant.

The fact that observed vesicles reveal the conformal invariance of  $G$  shows, that physical effects which break the conformal invariance are small. Two effects could be important. First, higher order curvature terms destroy the conformal invariance of the bending energy. Scaling arguments suggest these terms vanish for large vesicle sizes. A second effect comes from bending modes. The degeneracy of shapes along a conformal mode is broken since bending modes for different shapes along such a mode have different spectra which leads to different contributions to the free energy. This effect is expected to become important for large vesicle sizes where more bending modes exist. These arguments suggest that phospholipid vesicles are optimal in the sense that conformal invariance is preserved: They are sufficiently large to avoid that higher order curvature terms become relevant and they are at the same time sufficiently small, thus suppressing symmetry breaking contributions from bending modes to the free energy.

Vesicles therefore provide a unique system to realize the Willmore functional and to generate Willmore surfaces as observable structures. The observation of these Willmore-vesicles provides an experimental confirmation of Kusner's conjecture for which no mathematical proof is known. The only clear evidence for its validity comes from numerical computer "experiments" [29] and, as suggested here, from the experimental observation of vesicle shapes.

## Acknowledgments

I thank Udo Seifert, Reinhard Lipowsky, Wolfgang Wintz, Xavier Michalet, David Bensimon, Bertrand Fourcade and Paul Lammert for many discussions and the Max-Planck-Institut für Kolloid- und Grenzflächenforschung, where part of this manuscript was written, for its hospitality. This work was part of my PhD thesis which I did with Reinhard Lipowsky.

## Appendix A

### Geometry and Topology of Curved Surfaces

This section defines the notation used to describe curved surfaces embedded in Euclidean space  $R^3$  and the unit sphere  $S^3$ . The conformal invariance of the Willmore functional, the properties of stereo-graphic projections and the Gauss-Bonnet theorem are briefly reviewed.

A.1. SURFACES IN  $R^3$ . — A curved surface can be represented by a parameterization  $\mathbf{R}(s^1, s^2)$  of a vector  $\mathbf{R} = (R_1, R_2, R_3) = (X, Y, Z)$  with two internal coordinates  $s^1, s^2$ . Two tangent vectors

$$\partial_i \mathbf{R} \equiv \frac{\partial}{\partial s^i} \mathbf{R} \quad \text{with } i = 1, 2 \quad , \quad (\text{A.1})$$

allow to define the normal vector

$$\mathbf{n} \equiv \frac{\partial_1 \mathbf{R} \times \partial_2 \mathbf{R}}{|\partial_1 \mathbf{R} \times \partial_2 \mathbf{R}|} \quad . \quad (\text{A.2})$$

The metric tensor

$$g_{ij} \equiv \partial_i \mathbf{R} \cdot \partial_j \mathbf{R} \quad (\text{A.3})$$

characterizes the local geometry of the surface. The area element reads  $dA \equiv \sqrt{g} ds^1 ds^2$ , where  $g \equiv \det(g_{ij})$  denotes the determinant of the metric tensor. The curvature of the surface is characterized by the curvature tensor  $h_i^j$  defined by

$$\partial_i \mathbf{n} = h_i^j \partial_j \mathbf{R} \quad . \quad (\text{A.4})$$

It can be calculated using the relation

$$h_{ij} \equiv -(\partial_i \partial_j \mathbf{R}) \cdot \mathbf{n} \quad . \quad (\text{A.5})$$

The principal curvatures  $C_1$  and  $C_2$  are the eigenvalues of  $h_i^j = h_{ik} g^{kj}$ , where  $g^{kj} = (g^{-1})_{kj}$ . The mean curvature

$$H \equiv \frac{1}{2} \text{tr}(h_j^i) = \frac{1}{2} (C_1 + C_2) \quad , \quad (\text{A.6})$$

and the Gaussian curvature

$$K = \det(h_j^i) = C_1 C_2 \quad , \quad (\text{A.7})$$

are given by the trace and the determinant of the curvature tensor [46].

**A.2. CONFORMAL INVARIANCE OF THE WILLMORE FUNCTIONAL.** — The conformal invariance of the Willmore functional  $G$  as given by equation (8) is demonstrated following [20]. The invariance of  $G$  with respect to rotations, translations and scale transformations is obvious. It is therefore sufficient to show the invariance with respect to an inversion  $\mathbf{R}' = \mathbf{R}/R^2$  with

$$T_{\alpha\beta} \equiv \frac{\partial R'_\alpha}{\partial R_\beta} = \frac{1}{R^2} \left( \delta_{\alpha\beta} - 2 \frac{R_\alpha R_\beta}{R^2} \right) \quad . \quad (\text{A.8})$$

Since

$$T_{\alpha\beta} T_{\beta\gamma} = \frac{1}{R^4} \delta_{\alpha\gamma} \quad , \quad (\text{A.9})$$

the metric tensor and the area element transform as  $g'_{ij} = g_{ij}/R^4$  and  $dA' = dA/R^4$ . The transformation of the curvature tensor can be calculated using equation (A.8) and  $n'_\alpha = R^2 T_{\alpha\beta} n_\beta$ . It can be written as

$$h_j^{i'} = -R^2 h_j^i - 2(\mathbf{Rn}) \delta_j^i \quad . \quad (\text{A.10})$$

The transformation properties of the principal curvatures  $C_1$  and  $C_2$  follow using a coordinate system where  $h_i^j$  is diagonal:

$$C'_i = -R^2 C_i - 2(\mathbf{Rn}) \quad . \quad (\text{A.11})$$

Therefore,

$$(C'_1 - C'_2)^2 = R^4 (C_1 - C_2)^2 \quad . \quad (\text{A.12})$$

Together with the definitions (A.6) and (A.7), it follows that  $(H^2 - K)dA$  is conformally invariant. Since the topology of a closed surface does not change, one obtains using the Gauss-Bonnet theorem (A.35) that

$$\oint H'^2 dA' = \oint H^2 dA \quad . \quad (\text{A.13})$$

The Willmore functional therefore is invariant under conformal transformations of a closed surface [20, 31, 32].

A.3. SURFACES EMBEDDED IN  $S^3$ . — The 4-dimensional unit sphere  $S^3$  is defined as

$$S^3 = \{\underline{\mathbf{x}} = (x, y, z, w) \in R^4 \mid \underline{\mathbf{x}} \cdot \underline{\mathbf{x}} = x^2 + y^2 + z^2 + w^2 = 1\} \quad . \quad (\text{A.14})$$

Underlined letters denote vectors in  $R^4$  and the dot denotes the Euklidean scalar product in  $R^4$ . It is useful to choose coordinates  $\tilde{R}_1, \tilde{R}_2$  and  $\tilde{R}_3$  in  $S^3$  with  $\tilde{R}_1 = x, \tilde{R}_2 = y, \tilde{R}_3 = z$  and  $\tilde{R}_1^2 + \tilde{R}_2^2 + \tilde{R}_3^2 < 1$ . In this coordinate system,  $w = (1 - \tilde{R}_1^2 - \tilde{R}_2^2 - \tilde{R}_3^2)^{1/2}$ . The  $R^4$  imposes a natural metric on the  $S^3$  with

$$ds^2 = dx^2 + dy^2 + dz^2 + dw^2 = \tilde{G}^{\alpha\beta} d\tilde{R}_\alpha d\tilde{R}_\beta \quad . \quad (\text{A.15})$$

Here,

$$\tilde{G}^{\alpha\beta} = \underline{\mathbf{x}}^\alpha \cdot \underline{\mathbf{x}}^\beta = \delta_{\alpha\beta} + \frac{\tilde{R}_\alpha \tilde{R}_\beta}{w^2} \quad , \quad (\text{A.16})$$

is the metric tensor and the vectors

$$\underline{\mathbf{x}}^\alpha \equiv \partial^\alpha \underline{\mathbf{x}} \equiv \frac{\partial}{\partial \tilde{R}_\alpha} \underline{\mathbf{x}} \quad , \quad (\text{A.17})$$

span the 3-dimensional tangent space at a given point of  $S^3$ .

A surface embedded in  $S^3$  is described by a parameterization  $\underline{\mathbf{x}}(s^1, s^2)$  with  $\underline{\mathbf{x}} \cdot \underline{\mathbf{x}} = 1$ . Alternatively, a parameterization  $\tilde{R}_\alpha(s^1, s^2)$  of the coordinates  $\tilde{R}_\alpha$  can be used. The metric tensor of this surface is given by

$$\tilde{g}_{ij} \equiv \partial_i \underline{\mathbf{x}} \cdot \partial_j \underline{\mathbf{x}} = \tilde{G}^{\alpha\beta} \partial_i \tilde{R}_\alpha \partial_j \tilde{R}_\beta \quad , \quad (\text{A.18})$$

and the area element reads  $d\tilde{A} \equiv \sqrt{\tilde{g}} ds^1 ds^2$ , where  $\tilde{g} \equiv \det(\tilde{g}_{ij})$ . The normal vector  $\underline{\mathbf{n}} \in R^4$  with  $\underline{\mathbf{n}} \cdot \underline{\mathbf{n}} = 1$  is orthogonal to the surface, *i.e.*  $\underline{\mathbf{n}} \cdot \partial_i \underline{\mathbf{x}} = 0$ , and it is tangential to  $S^3$ , *i.e.*  $\underline{\mathbf{n}} \cdot \underline{\mathbf{x}} = 0$ . It can be expressed as  $\underline{\mathbf{n}} = \tilde{n}_\alpha \underline{\mathbf{x}}^\alpha$ .

The curvature tensor  $\tilde{h}_i^j$  of a surface in  $S^3$  can be defined as [33]

$$\partial_i \underline{\mathbf{n}} = \tilde{h}_i^j \partial_j \underline{\mathbf{x}} \quad . \quad (\text{A.19})$$

It can be calculated according to

$$\tilde{h}_{ij} \equiv -(\partial_i \partial_j \underline{\mathbf{x}}) \cdot \underline{\mathbf{n}} = -\tilde{G}^{\alpha\beta} \tilde{n}_\beta \partial_i \partial_j \tilde{R}_\alpha - \partial_i \tilde{R}_\gamma \partial_j \tilde{R}_\alpha \Gamma^{\alpha\beta\gamma} \tilde{n}_\beta \quad . \quad (\text{A.20})$$

Here,

$$\Gamma^{\alpha\beta\gamma} \equiv (\partial^\gamma \underline{\mathbf{x}}^\alpha) \cdot \underline{\mathbf{x}}^\beta = \frac{1}{2} \left( \partial^\gamma \tilde{G}^{\alpha\beta} + \partial^\alpha \tilde{G}^{\gamma\beta} - \partial^\beta \tilde{G}^{\alpha\gamma} \right) \quad , \quad (\text{A.21})$$

are the Christoffel symbols of the metric  $\tilde{G}^{\alpha\beta}$ . The mean curvature  $\tilde{H}$  is again given by the trace of the curvature tensor

$$\tilde{H} \equiv \frac{1}{2} \text{tr}(\tilde{h}_j^i) \quad . \quad (\text{A.22})$$

The determinant of the curvature tensor

$$\tilde{K} \equiv \det(\tilde{h}_j^i) \quad , \quad (\text{A.23})$$

is the *extrinsic curvature* [30] which differs from the Gaussian curvature  $\bar{K}$  (see Sect. A.5).

A.4. STEREO-GRAPHIC PROJECTIONS. — The properties of stereo-graphic projections of surfaces in  $S^3$  are briefly reviewed. These properties are used in Section C to demonstrate the relation between minimal surfaces in  $S^3$  and Willmore surfaces. A stereo-graphic projection maps a point  $\underline{x}(\tilde{R}_1, \tilde{R}_2, \tilde{R}_3)$  in  $S^3$  onto a point  $\mathbf{R} = (R_1, R_2, R_3)$  in  $R^3$ . The transformation is defined by

$$R_\alpha = \frac{\tilde{R}_\alpha}{(1+w)} \quad . \quad (\text{A.24})$$

The derivative matrix

$$\Lambda_\alpha^\beta \equiv \frac{\partial R_\alpha}{\partial \tilde{R}_\beta} = \frac{1}{1+w} \left( \delta_{\alpha\beta} + \frac{\tilde{R}_\alpha \tilde{R}_\beta}{w(1+w)} \right) \quad , \quad (\text{A.25})$$

obeys

$$\Lambda_\alpha^\beta \Lambda_\alpha^\gamma = \frac{1}{(1+w)^2} \tilde{G}^{\beta\gamma} \quad . \quad (\text{A.26})$$

Therefore, the metric tensor transforms as

$$g_{ij} = \frac{1}{(1+w)^2} \tilde{g}_{ij} \quad . \quad (\text{A.27})$$

The fact that  $\tilde{g}_{ij}$  is multiplied by a scalar implies that the stereo-graphic projection is conformal. Similarly, the transformation of the area element reads

$$dA = \frac{1}{(1+w)^2} d\tilde{A} \quad . \quad (\text{A.28})$$

The normal vector transforms as  $n_\alpha = (1+w)\Lambda_\alpha^\beta \tilde{n}_\beta$ . This follows from the fact that the stereo-graphic projection is conformal and conserves angles. The factor  $(1+w)$  normalizes  $n_\alpha n_\alpha = 1$ . The transformation of the curvature tensor can be calculated using

$$h_{ij} = -(\partial_i \partial_j R_\alpha) n_\alpha = -\frac{1}{1+w} \tilde{G}^{\alpha\beta} \tilde{n}_\beta \partial_i \partial_j \tilde{R}_\alpha - (1+w) \partial_i \tilde{R}_\gamma \partial_j \tilde{R}_\alpha (\partial^\gamma \Lambda_\delta^\alpha) \Lambda_\delta^\beta \tilde{n}_\beta \quad . \quad (\text{A.29})$$

Together with equation (A.20) and inserting equation (A.26) in equation (A.21) one finds

$$h_i^j = (1+w) \tilde{h}_i^j + \delta_i^j \tilde{n}_\alpha \partial^\alpha (1+w) \quad . \quad (\text{A.30})$$

Following the same argumentation as outlined in Section A.2, it follows that

$$\int_{R^3} dA (H^2 - K) = \int_{S^3} d\tilde{A} (\tilde{H}^2 - \tilde{K}) \quad . \quad (\text{A.31})$$

This is another example of the conformal invariance of  $(H^2 - K)dA$ .

A.5. THE GAUSS-BONNET THEOREM. — The Gaussian curvature  $\bar{K}$  can be calculated from the metric tensor  $g_{ij}$  and its first and second derivatives alone. In a coordinate system, where the metric tensor is diagonal the Gaussian curvature can be defined as [46]

$$\bar{K} \equiv -\frac{1}{\sqrt{g_{11}g_{22}}} \left[ \partial_1 \left\{ \frac{1}{\sqrt{g_{11}}} \partial_1 \sqrt{g_{22}} \right\} + \partial_2 \left\{ \frac{1}{\sqrt{g_{22}}} \partial_1 \sqrt{g_{11}} \right\} \right] \quad . \quad (\text{A.32})$$

This definition can be used for surfaces in  $R^3$  as well as in  $S^3$ . For a surface embedded in  $R^3$ ,  $\bar{K}$  can also be expressed by the determinant of the curvature tensor:

$$\bar{K} = K = \det(h_i^j) \quad . \quad (\text{A.33})$$

This expression is not correct for a surface in  $S^3$  for which

$$\bar{K} = \tilde{K} + 1 = \det(\tilde{h}_i^j) + 1 \quad . \quad (\text{A.34})$$

This difference comes from the fact that  $S^3$  has constant curvature itself which in addition to the extrinsic curvature contributes to the Gaussian curvature  $\bar{K}$ .

The Gauss-Bonnet theorem states that

$$\oint dA \bar{K} = 4\pi(1 - g) \quad , \quad (\text{A.35})$$

only depends on the topology of the surface characterized by its topological genus  $g$  [46]. For a surface embedded in  $S^3$ , the Gauss-Bonnet theorem can thus be expressed as [30]

$$\oint_{S^3} d\tilde{A} (\tilde{K} + 1) = 4\pi(1 - g) \quad . \quad (\text{A.36})$$

## Appendix B

### Minimal Surfaces in $S^3$

B.1. GENERAL PROPERTIES. — A minimal surface has extremal surface area, *i.e.*  $\delta\tilde{A}$  vanishes for arbitrary variations

$$\underline{\mathbf{x}}'(s^1, s^2) = \underline{\mathbf{x}}(s^1, s^2) + \tilde{\epsilon}(s^1, s^2) \underline{\mathbf{n}}(s^1, s^2) \quad , \quad (\text{B.1})$$

of a surface in  $S^3$ , where  $\tilde{\epsilon}(s^1, s^2) \ll 1$ . Under this deformation, the metric tensor becomes

$$\tilde{g}'_{ij} = \tilde{g}_{ij} + \tilde{\epsilon}(\partial_i \underline{\mathbf{x}} \cdot \partial_j \underline{\mathbf{n}} + \partial_j \underline{\mathbf{x}} \cdot \partial_i \underline{\mathbf{n}}) + O(\tilde{\epsilon}^2) \quad . \quad (\text{B.2})$$

With the identity  $\det(\delta_i^j + \epsilon a_i^j) = 1 + \epsilon \text{Tr}(a_i^j) + \epsilon^2 \det(a_i^j)$ , it follows that

$$\tilde{g}' = (1 + 4\tilde{\epsilon}\tilde{H})\tilde{g} + O(\tilde{\epsilon}^2) \quad , \quad (\text{B.3})$$

and the variation of the surface area reads

$$\delta\tilde{A} = 2 \oint d\tilde{A} \tilde{H} \tilde{\epsilon} + O(\tilde{\epsilon}^2) \quad . \quad (\text{B.4})$$

A minimal surface in  $S^3$  therefore obeys  $\tilde{H} = 0$  everywhere [47].

B.2. FAMILIES OF MINIMAL SURFACES. — Different families of closed minimal surfaces in  $S^3$  have been discovered by Lawson [33]. These families are denoted  $\xi_{kn}$ ,  $\eta_{kn}$  and  $\tau_{kn}$ , where  $k$  and  $n$  are integers. The topological genus of these surfaces is  $g = kn$ . More recently, additional minimal surfaces have been described by Karcher, Pinkall and Sterling [34].

These minimal surfaces in  $S^3$  have in common that they consist of a set of surface patches of extremal surface area, bounded by geodesic lines. The net of boundary geodesics defines a minimal surface and determines its symmetry properties [33].

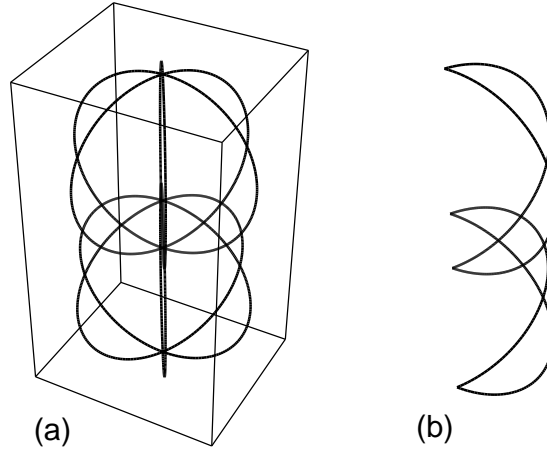


Fig. 12. — (a) The lines  $A_{pq}$  of the minimal surface  $\xi_{12}$  stereo-graphically projected to  $R^3$ . A unit cell of this network is shown in (b). For details, see text.

For the surfaces  $\xi_{1g}$  with  $k = 1$  and  $n = g$ , the set of boundary geodesics can be written as

$$A_{pq} = \{ \mathbf{x}(\theta, \phi, \psi) \mid \phi = q\pi/2, \quad \theta = p\pi/(g + 1), \quad 0 \leq \psi \leq \pi/2 \} \quad , \quad (\text{B.5})$$

with integers  $0 \leq p \leq 2g + 1$  and  $0 \leq q \leq 3$  [33]. Here, a point in  $S^3$  is characterized by three angular coordinates with

$$\begin{aligned} x &= \cos \theta \cos \psi \\ y &= \sin \theta \cos \psi \\ z &= \cos \phi \sin \psi \\ w &= \sin \psi \sin \phi \quad . \end{aligned} \quad (\text{B.6})$$

The stereo-graphic projection of the boundary geodesics  $A_{pq}$  of the surface  $\xi_{12}$  is shown in Figure 12. It consists of six pairs of circles that are arranged with sixfold symmetry. The complete net  $A_{pq}$  is  $\mathcal{D}_{6h}$ -symmetric. The genus-2 Lawson surface contains this net of boundary geodesics and is  $\mathcal{D}_{3h}$ -symmetric.

### Appendix C

#### Relation Between Willmore Surfaces and Minimal Surfaces

A closed surface in  $S^3$  can be mapped into  $R^3$  using the stereo-graphic projection (A.24). Using equation (A.31) and the Gauss-Bonnet theorem (A.36), one obtains

$$\oint_{R^3} dA H^2 = \oint_{S^3} d\tilde{A} (\tilde{H}^2 + 1) \quad . \quad (\text{C.1})$$

If this relation is applied to a minimal surface in  $S^3$  with  $\delta\tilde{A} = 0$  and vanishing mean curvature  $\tilde{H} = 0$ , it follows that [30–32]

$$G = \frac{\kappa}{2} \oint dA (2H)^2 = 2\kappa\tilde{A} \quad , \quad (\text{C.2})$$

*i.e.*,  $G$  is extremal for arbitrary deformations

$$\mathbf{R}'(s^1, s^2) = \mathbf{R}(s^1, s^2) + \epsilon(s^1, s^2) \mathbf{n}(s^1, s^2) \quad (\text{C.3})$$

in  $R^3$  which correspond to deformations described by equation (B.1) with  $\tilde{\epsilon} = (1+w)\epsilon + O(\epsilon^2)$  in  $S^3$ . Therefore,

$$\delta G = \kappa \oint_{S^3} d\tilde{A} \tilde{\epsilon} \tilde{H} \left( \tilde{H}^2 + 1 + 4 \frac{\delta \tilde{H}}{\delta \tilde{\epsilon}} \right) \quad (\text{C.4})$$

vanishes for a minimal surface with  $\tilde{H} = 0$ . The stereo-graphic projection of a minimal surface in  $S^3$  therefore is minimum or a saddle point of the Willmore functional [48].

## Appendix D

### Numerical Methods

D.1. TRIANGULATED SURFACES. — A smooth surface can be approximated by a polyhedron formed of triangles  $T_i$ , with  $i = 1, \dots, n_T$ . A given triangulation of a closed surface consists of  $n_T$  triangles,  $n_E$  edges and  $n_V$  vertices, with  $n_T - n_E + n_V = 2(1-g)$ , where  $g$  is the topological genus of the surface [49]. The total area of a triangulation can be calculated as

$$A = \sum_{i=1}^{n_T} A_i \quad , \quad (\text{D.1})$$

where  $A_i$  is the area of triangle  $T_i$ . The enclosed volume is given by

$$V = \sum_{i=1}^{n_T} V_i \quad , \quad (\text{D.2})$$

where

$$V_i \equiv \frac{1}{3} (\mathbf{n}_i \cdot \mathbf{R}_i) A_i \quad . \quad (\text{D.3})$$

Here,  $\mathbf{n}_i$  denotes the normal vector on triangle  $T_i$  and  $\mathbf{R}_i$  is the position of one of the edges of  $T_i$ . The total mean curvature can be written as

$$M = \frac{1}{2} \sum_{\langle ij \rangle} l_{ij} \phi_{ij} \quad , \quad (\text{D.4})$$

where the sum runs over triangles which are adjacent and  $l_{ij}$  is the length of the common edge of triangles  $T_i$  and  $T_j$ . The angle

$$\cos \phi_{ij} = \mathbf{n}_i \cdot \mathbf{n}_j \quad , \quad (\text{D.5})$$

is the angle between the normals  $\mathbf{n}_i$  and  $\mathbf{n}_j$  of adjacent triangles.

A discretization of the bending energy is more subtle. One way to define  $G$  on a triangulation is to first calculate the contribution  $M_\alpha$  of a vertex  $\alpha = 1, \dots, n_V$  to the total mean curvature  $M$ ,

$$M_\alpha \equiv \frac{1}{4} \sum_{\langle ij \rangle}^{(\alpha)} l_{ij} \phi_{ij} \quad , \quad (\text{D.6})$$

where the sum runs over all pairs of adjacent triangles which have the vertex  $\alpha$  in common. The factor  $1/4$  ensures that

$$M = \sum_{\alpha=1}^{n_V} M_{\alpha} \quad . \quad (\text{D.7})$$

The area element corresponding to vertex  $\alpha$  is given by

$$A_{\alpha} \equiv \frac{1}{3} \sum_{\langle i \rangle}^{(\alpha)} A_i \quad , \quad (\text{D.8})$$

where the sum runs over all triangles which share vertex  $\alpha$ . Now, the discretized bending energy can be written as

$$G = 2\kappa \sum_{\alpha=1}^{n_V} \frac{M_{\alpha}^2}{A_{\alpha}} \quad . \quad (\text{D.9})$$

**D.2. APPROXIMATION OF THE GENUS-2 LAWSON SURFACE.** — The approximated genus-2 Lawson surface as displayed in Figure 2 was obtained by numerically minimizing the discretized bending energy given by equation (D.9) using a gradient method. Since this method will in general lead to a local minimum, the proper choice of an initial configuration is important. Very useful for this purpose is the family  $\Xi_{1g}$  of surfaces of topological genus  $g$  embedded in  $S^3$ . This family of surfaces is defined by [33]

$$\Xi_{1g} = \{ \mathbf{x}(\theta, \phi, \psi) \mid \cos^{(g+1)} \psi \sin((g+1)\theta) + |\sin \psi|^{(g+1)} \sin 2\phi = 0 \} \quad , \quad (\text{D.10})$$

where the parameterization of  $S^3$  given by equation (B.6) is used. The surface  $\Xi_{1g}$  contains the lines  $A_{pq}$  given by equation (B.5). Furthermore,  $\Xi_{1g}$  has the same topology and the same symmetry as  $\xi_{1g}$ . The surface  $\Xi_{10} = \xi_{10}$  is the sphere and  $\Xi_{11} = \xi_{11}$  is the Clifford torus. For  $g > 1$  the surfaces  $\Xi_{1g}$  and  $\xi_{1g}$  are different except to the lines  $A_{pq}$ . Starting from the stereographic image of  $\Xi_{12}$  as initial condition, the Lawson surface can be generated by numerical energy minimization.

## References

- [1] Lipowsky R., *Nature* **349** (1991) 475.
- [2] Bloom M., Evans E. and Mouritsen O., *Q. Rev. Biophys.* **24** (1991) 293.
- [3] Berndt K., *et al.*, *Europhys. Lett.* **13** (1990) 659.
- [4] Käs J. and Sackmann E., *Biophys. J.* **60** (1991) 825.
- [5] Evans E. and Rawicz W., *Phys. Rev. Lett.* **64** (1990) 2094.
- [6] Wiese W., Harbich W. and Helfrich W., *J. Phys.: Cond. Matter* **4** (1992) 1647.
- [7] Helfrich W., *Z. Naturforsch.* **28c** (1973) 693.
- [8] Evans E., *Biophys. J.* **14** (1974) 923.
- [9] Deuling H. and Helfrich W., *J. Phys. France* **37** (1976) 1335.
- [10] Svetina S. and Zeks B., *Eur. Biophys. J.* **17** (1989) 101.
- [11] Seifert U., Berndt K. and Lipowsky R., *Phys. Rev. A* **44** (1991) 1182.
- [12] Miao L., *et al.*, *Phys. Rev. A* **43** (1991) 6843.
- [13] Miao L., Seifert U., Wortis M. and Döbereiner H.-G., *Phys. Rev. E* **49** (1994) 5389.
- [14] Wintz W., Döbereiner H.-G. and Seifert U., *Europhys. Lett.* **33** (1996) 403.

- [15] Mutz M. and Bensimon D., *Phys. Rev. A* **43** (1991) 4525.
- [16] Fourcade B., Mutz M. and Bensimon D., *Phys. Rev. Lett.* **68** (1992) 2551.
- [17] Michalet X. and Bensimon D., *J. Phys. II France* **5** (1995) 263.
- [18] Michalet X., Bensimon D. and Fourcade B., *Phys. Rev. Lett.* **72** (1994) 168.
- [19] Michalet X. and Bensimon D., *Science* **269** (1995) 666.
- [20] Willmore T., Total curvature in Riemannian geometry (Ellis Horwood, Chichester, 1982).
- [21] Duplantier B., *Physica A* **168** (1990) 179.
- [22] Duplantier B., Goldstein R., Romero-Rochin V. and Pesci A., *Phys. Rev. Lett.* **65** (1990) 508.
- [23] Seifert U., *Phys. Rev. Lett.* **66** (1991) 2404.
- [24] Seifert U., *J. Phys. A: Math. Gen.* **24** (1991) L573.
- [25] Fourcade B., *J. Phys. II France* **2** (1992) 1705.
- [26] Jülicher F., Seifert U. and Lipowsky R., *J. Phys. II France* **3** (1993) 1681.
- [27] Jülicher F., Seifert U. and Lipowsky R., *Phys. Rev. Lett.* **71** (1993) 452.
- [28] Pinkall U. and Sterling I., *Math. Intelligencer* **9** (1987) 38.
- [29] Hsu L., Kusner R. and Sullivan J., *Experimental Math.* **1** (1992) 191.
- [30] Kusner R., *Pacific J. Math.* **138** (1989) 317.
- [31] Thomsen G., *Abh. Math. Sem. Univ. Hamburg* **3** (1923) 31.
- [32] Blaschke W., Vorlesungen über Differentialgeometrie (Springer, Berlin, 1929).
- [33] Lawson H., *Ann. Math.* **92** (1970) 335.
- [34] Karcher H., Pinkall U. and Sterling I., *J. Differential Geometry* **28** (1988) 169.
- [35] Willmore T., *Anal. Scient. ale Univ. Iasi (Sect. Ia)* **11** (1965) 493.
- [36] Note that definition (9) differs from those used in references [24,26] by a minus sign.
- [37] Ashcroft N. and Mermin N., Solid State Physics (CBS Publishing Asia Ltd., Philadelphia, 1976).
- [38] This “handle” has two holes since the limit shape is of topological genus  $g = 2$ .
- [39] Note that no additional Willmore surfaces can be generated by using inversion centers located in the exterior of  $L$ . This fact follows from the inversion symmetry of  $L$ .
- [40] The limit  $|\mathbf{a}| \rightarrow \infty$  leads to the Lawson surface which is not part of any conformal mode.
- [41] Brochard F. and Lennon J., *J. Phys. France* **36** (1975) 1035.
- [42] Evans E. and Needham D., *J. Phys. Chem.* **91** (1987) 4219.
- [43] Duwe H., Käs J. and Sackmann E., *J. Phys. France* **51** (1990) 945.
- [44] Mutz M. and Helfrich W., *J. Phys. France* **51** (1990) 991.
- [45] All known surfaces which are solutions of curvature models for vesicle shapes have at least two mirror planes and obey equation (31) by symmetry. In principle,  $C_{2h}$ -symmetry would be sufficient to satisfy equation (31) ( $C_{2h}$ -symmetry corresponds to a two-fold axis and an additional mirror plane perpendicular to this axis.).
- [46] do Carmo M., Differential Geometry of Curves and Surfaces (Prentice-Hall, New Jersey, 1976).
- [47] Nitsche J., Lectures on minimal surfaces (Cambridge University Press, Cambridge, 1989).
- [48] Equation (C.4) shows that any surface which obey  $\tilde{H}^2 + 1 + 4\delta\tilde{H}/\delta\tilde{\epsilon} = 0$ , is also a stationary solution of the Willmore functional with  $\delta G = 0$ . However, no surface with  $\delta G = 0$  is known which does not correspond to a minimal surface [28].
- [49] Spivak M., Differential Geometry (Publish or Perish, Houston, 1979).